L03

Proceedings of the 5th International Conference on Inverse Problems in Engineering: Theory and Practice, Cambridge, UK, 11-15th July 2005

MODEL SELECTION IN HYDRAULIC FRACTURE IMAGING FROM ELASTOSTATIC MEASUREMENTS

B. LECAMPION and J. GUNNING
CSIRO Petroleum, Melbourne Office, PB 10, Clayton South, Vic. 3169, Australia
e-mail: Brice.Lecampion@csiro.au, James.Gunning@csiro.au

Abstract - In this paper, the imaging of hydraulic fractures from tilt measurements is investigated with regards to model selection. The quantitative selection of the most probable model in a finite set of fracture geometry and loading is carried out using Bayes factors. The modeling error variance is also estimated during the inversion procedure. Such model selection method allows to retrieve a known limit for the resolution of fracture dimensions depending on the measurements configuration. Synthetic as well as field examples are presented.

1. INTRODUCTION

Hydraulic fracturing is a technique routinely used in the petroleum industry to enhance the productivity of wells [5]. It consists of injecting a viscous fluid under high pressure in order to propagate a fracture from the well into the formation. In the latter stage of a treatment, a mixture of sand is added to the fracturing fluid. This has the effect of creating a highly permeable channel when the fracture closes back on itself, thus eventually enhancing oil recovery. The propagation of a hydraulic fracture is a highly non-linear process due to the coupling between the viscous flow inside the fracture, the elasticity equation, fracture propagation conditions, and fluid leak-off into the formation. Depending on the configuration (injection rates, fluid rheology, rock properties etc.), the length and width of the created fracture can vary by orders of magnitudes. The mapping of such planar fractures (orientation, dimensions) is a critical issue for reservoir management purposes. Unfortunately, no direct measurement of the created fracture is currently possible, so the success of a treatment can only be assessed after production has restarted. In the last few decades different monitoring techniques have been developed to image hydraulic fractures. The most popular are acoustic emission and tiltmeter monitoring. In this paper, we are interested in the use of tiltmeter measurements for inferring relevant characteristics of the created fracture.

Tiltmeters measure the quasi-static change of inclination due to the pressurization and propagation of the hydraulic fracture. In petroleum applications, a typical measurement array would consist of *at most* a dozen tiltmeters located either on the earth's surface or in a monitoring borehole (see Figure 1 for a typical set-up). The goal is to obtain from such elastostatic data the orientation and dimensions of the created fracture. Unfortunately, due to the elliptic character of quasi-static elasticity, the geometric signatures of the fracture get "blurred" very quickly as the distance between the measurement location and the fracture increases (St Venant's principle). In the far-field, the fracture becomes equivalent to a Displacement Discontinuity Singularity (i.e. a dislocation dipole), which simplifies the modeling, but only fracture orientation and volume can be estimated. When measurements are located in the near-field, the shape of the fracture has an important effect and the choice of the fracture model (geometry, internal pressure) becomes crucial.

The problem of fracture detection from elasto-static measurement has been investigated mainly in the context of damage identification [1]. Our problem has important differences. The crack is pressurized and this pressure is unknown. Also, unlike the case of non destructive testing, we cannot control the loading on the boundary to better resolve the fracture; we have only one set of data, at very few points inside the medium, corresponding to the propagation of the fracture. In practice, one has also to remember that the hydraulic fracture is located in a rock mass that can be rather inhomogeneous and whose elastic properties are often poorly known. Even when the measurements are known to be located in the near-field pattern of the fracture, the use of a complete mesh to model the fracture is more or less prohibited by the unknown orientation of the fracture plane, and the limited measurements available. It is more pragmatic, for engineering purposes, to use a simple fracture model (radial or elliptical crack, square Displacement Discontinuity, single Displacement Discontinuity singularity...) to analyze the data, although all these models may be *incorrect*. Within this scope, it is natural to investigate the problem of model selection and model uncertainty. The Bayesian approach to inverse problems is well suited to quantitatively handle

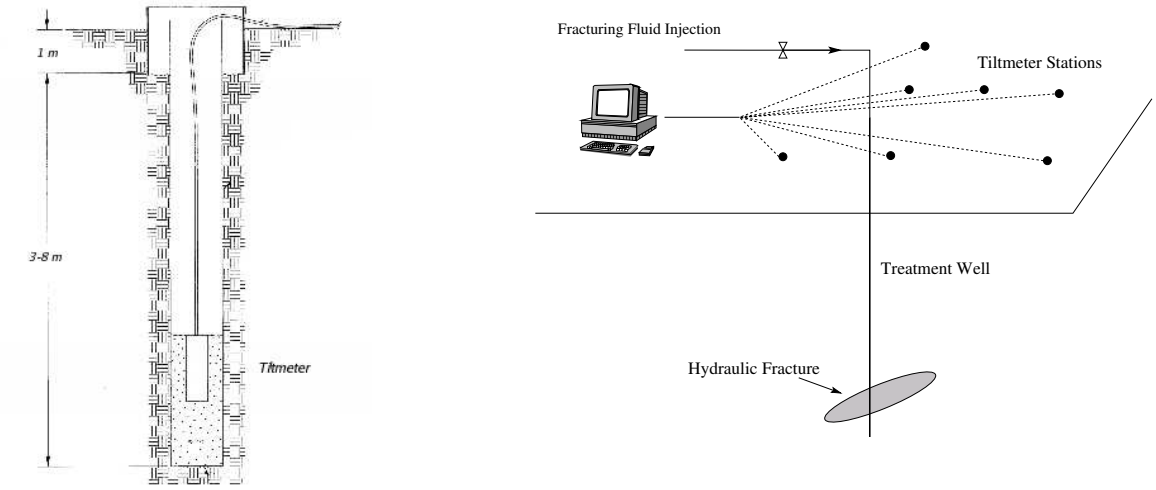

Figure 1. Set-up of tiltmeter in shallow boreholes (left, After `Geomechanics Inc.`), and typical layout of a measurement array for fracture monitoring (right).

this class of problems. Model selection problems have received a considerable interest in the last decade in the statistical and social science communities. Engineering applications are less frequent: one can cite, among others, [12] in the case of electrical imaging, [2] in structural mechanics.

In this paper, we use a Bayesian approach to rank several different possible fracture models for the typical non-linear inverse problem of hydraulic fracture imaging. The details of the method are discussed. A synthetic example shows the benefits of such an approach, especially in relation to the far-field/near-field fracture resolution problem. Real tiltmeter data from a full scale hydraulic fracturing treatment are also inverted and different possible fracture geometries are tested.

2. PROBLEM DESCRIPTION

2.1 Tiltmeter fracture mapping

Modern high precision tiltmeters can detect changes of inclination down to nanoradians, which makes possible the monitoring of deep pressurized fractures. Several types of tilt sensor exist, but the most common are electrolyte level sensors, which convert changes of tilt angle to changes of resistance. The sensor measures the angle between its axis and the gravity vector. Most instruments are equipped with 2 such sensors, one for each axis of tilt. The tiltmeter in itself is a rigid body and also contains signal processing electronics. Usually for geotechnical applications, tiltmeters are located in shallow boreholes (several meters deep) in order to reduce the ambient noise. A typical set up of an instrument is depicted in Figure 1. In that case, the tiltmeter can be assumed to be fully clamped to the surrounding rock. A similar coupling is obtained if the instrument is fixed to an existing well-bore using mechanical arms. The angles recorded are related to the infinitesimal rotation at the instrument point. The two recorded tilts (along the two orthogonal axis (e_1, e_2) of the instrument) are related to two components of the so-called rotation tensor in small strain $\boldsymbol{w} = \frac{1}{2}\left(\boldsymbol{\nabla u} - \boldsymbol{\nabla}^T \boldsymbol{u}\right)$:

$$\alpha_1 = w_{31} = \frac{1}{2}\left(\frac{\partial u_3}{\partial x_1} - \frac{\partial u_1}{\partial x_3}\right) \qquad \alpha_2 = w_{32} = \frac{1}{2}\left(\frac{\partial u_3}{\partial x_2} - \frac{\partial u_2}{\partial x_3}\right)$$

Typically, a dozen instruments or so are used in hydraulic fracturing applications. A schematic view of a typical surface array can be seen in Figure 1. Downhole tiltmeter arrays located in the monitoring well (or even the treatment well) are also used in the industry. Prior to any inversion procedure, the tilt data have to be corrected for the effect of earth tides (particularly for surface tiltmeters) and any instrumental drift. Figure 2 displays the two corrected tilts recorded by a tiltmeter during a real hydraulic fracturing treatment. The change of tilt induced by the propagation of the hydraulic fracture can be clearly seen, as well as the beginning of the return of the tilt toward zero after the end of the injection. This return is delayed due to the diffusion of fracturing fluid in the rock mass.

The change of tilt between the beginning of the injection and a particular time t_i, obtained at several points in the medium, provides accurate data for an inverse problem for the fracture geometry. This

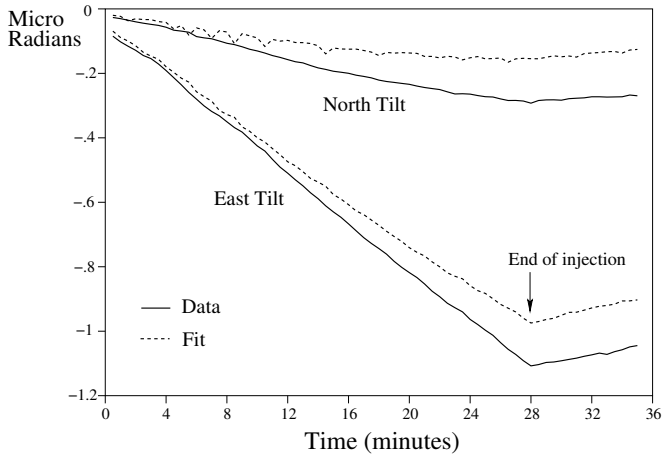

Figure 2. Field experiment: typical evolution of tilt data during a Hydraulic fracturing treatment. The corresponding best fit is also displayed.

inverse problem is sequentially solved at different times during the injection period in order to monitor the growth of the hydraulic fracture.

2.2 The forward and inverse problems

The elastostatic deformation and tilts induced by a pressurized fracture S are solution of the following elastostatic boundary value problem in the domain Ω:

$$\begin{aligned} \operatorname{div} \boldsymbol{C} : \boldsymbol{\varepsilon}(\boldsymbol{u}) &= \mathbf{0} \quad \text{in } \Omega \backslash S \\ \boldsymbol{T}(\boldsymbol{u}) \cdot \boldsymbol{n} &= p(x) \quad \text{on } S \end{aligned} \tag{1}$$

where $\boldsymbol{C}$ is the tensor of elastic moduli, $\boldsymbol{u}$ the displacement field, and $\boldsymbol{\varepsilon}$ the small strain operator $\boldsymbol{\varepsilon}(\boldsymbol{u}) = \frac{1}{2}(\boldsymbol{\nabla u} + \boldsymbol{\nabla}^T \boldsymbol{u})$. The traction vector is defined as $\boldsymbol{T} = \boldsymbol{\sigma} \cdot \boldsymbol{n}$. In our case, we will consider only a half-space or full-space domain such that the additional boundary conditions are:

- in the half-space case, a traction–free surface on the surface of the half-plane, and vanishing displacement and stress at infinite depth,
- in the case of the infinite medium, vanishing displacement and stress at infinity.

We note that the internal fracture loading can also be represented as a displacement jump $[D]$ of the fracture faces. This forward problem can be recast in the framework of eigenstrain theory, so the displacements, stresses and tilts can be obtained by a superposition of Displacements Discontinuity Singularities (see [8]). For example, the displacement in the case of the opening mode fracture can be expressed as

$$u_i(\boldsymbol{x}) = \int_S U_{ijk}(\boldsymbol{x}, \boldsymbol{x'}) n_j n_k D_n(\boldsymbol{x'}) \, \mathrm{d}\boldsymbol{x'} \tag{2}$$

In our notation, $(U_{ijk} \cdot D_{jk})$ denotes the displacement u_i at $\boldsymbol{x}$ induced by a DD singularity of the form D_{jk} located at $\boldsymbol{x'}$. $(D_{jk} \cdot n_k)$ represents a displacement jump across an element oriented by its unit normal n_k. We define $D_n = D_{ij} n_i n_j$ as the normal component of the displacement jump. A similar integral representation exists for the displacement gradient and therefore the tilts. We note that the fundamental kernel U_{ijk} is regular everywhere except on the fracture ($\boldsymbol{x} = \boldsymbol{x'}$). In the case of fracture monitoring, the instruments are located outside the fracture domains, simplifying the evaluation of the integral (2).

For a given time, the inverse problem consists in finding the fracture dimensions, the orientation (S, $\boldsymbol{n}$) and the opening profile $D_n(\boldsymbol{x'})$ from observations of the tilts w_{31}, w_{32} at $N/2$ different tiltmeter stations in the medium. These data forms an observation vector $\boldsymbol{d}$ of length N.

Before discussing the solution of this problem, it is important to recall a result recently obtained regarding the resolution of fracture dimensions from such measurements [11]. It can be shown that the details of the fracture shape get attenuated very quickly as the distance between the measurements and the fracture increases. This is a typical consequence of St Venant's principle in elasticity. It is

possible to prove that a severe non-uniqueness for the fracture dimensions exists in the case of far-field measurement. Observations located in the far-field deformation pattern of a pressurized fracture are only sensitive to the volume and orientation of the fracture: in the far-field the fracture is equivalent to a Displacement Discontinuity Singularity with an intensity equal to the fracture volume. In the case of near-field measurements, the shape as well as the internal pressure of the fracture start to have a visible effect on the deformation field. The far-field/near-field transition has been estimated using a far-field expansion in terms of the fracture length of a finite fracture solution in a full-space [11]. The far-field non-uniqueness on fracture dimensions becomes strong when the measurements are located at a distance greater than twice the fracture characteristic length ℓ. This result is extremely important in practice, as the measurements are often far from the fracture with respect to its length. In practice, we distinguish between two case: near-field and far-field tiltmeter fracture mapping, dependent on the location of the measurement and the expected size of the fracture.

For far-field fracture mapping, a simple DD Singularity model (i.e $U_{ijk}(\boldsymbol{x}, \boldsymbol{x'})n_j n_k$) with an intensity equal to the fracture volume can be used to robustly invert the data and obtain the fracture volume and orientation. For near-field tiltmeter mapping, the dimensions of the fracture may be resolved but the choice of the proper geometrical model becomes crucial. As mentioned in the introduction, the unknown orientation of the fracture plane and the small number of measurements prohibits the use of a discretization (using boundary elements for example) of a large finite surface in order to obtain a finite linear inverse problem for the opening at each node. Moreover, it is difficult to know a priori the characteristic length ℓ of the created fracture, so we never really know if we are in a case of near-field or far-field fracture mapping. In the far-field case, the severe non-uniqueness prevents us from using a complex discretization to invert the integral eqn.(2). It is more practical for engineering purpose to use simple fracture geometries in order to analyse the data. Using such simple parametrizations of the fracture, with analytical expressions for the tilts, enables much faster solution of the inverse problem. This ultimately allows real-time estimation – during the fracture treatment – of some fracture parameters. We can, if needed, increase the complexity of the model incrementally.

Along these lines, in the near-field case, the choice of the best model from a finite set of fracture geometries becomes a crucial problem. We use a Bayesian model selection approach to treat the problem quantitatively. For a model $\mathcal{M}_k$, the data $\boldsymbol{d}$ recorded at time t_i can be formally represented as:

$$\boldsymbol{d} = \boldsymbol{g}_k(\boldsymbol{m}_k) + \boldsymbol{\epsilon}_k \tag{3}$$

where $\boldsymbol{g}_k$ is the model function simulating the tilt. In the case of fracture detection, $\boldsymbol{g}_k$ is a non linear function of the parameters $\boldsymbol{m}_k$ of the model $\mathcal{M}_k$. The model parameter vector $\boldsymbol{m}_k$ is finite and contains the fracture orientation (with normal $\boldsymbol{n}$ defined by Euler angles), size parameters etc. The noise vector $\boldsymbol{\epsilon}_k$ incorporates the experimental and modelling noise for the model $\mathcal{M}_k$. This noise depends on the chosen model (i.e: modelling error) and *is an unknown to be estimated*. For simplicity, we assume that $\boldsymbol{\epsilon}_k$ is Gaussian of zero-mean and variance σ_k^2: $\boldsymbol{\epsilon}_k = \mathcal{N}(0, \sigma_k^2 \boldsymbol{I})$. The underlying assumptions of this choice is that the error is the same for all data points and that there is no spatial correlation in the error.

Given the data set $\boldsymbol{d}$ at time t_i, we want to estimate, among a set of pre-supposed models $\mathcal{M}_k$, $k = 1, 2, ...$ the most probable model as well as the corresponding model parameters $\boldsymbol{m}_k$ and model noise variance σ_k^2. To achieve this, we solve an inverse problem for each model and then use a Bayesian criterion to rank the different models. This is repeated sequentially in time in order to cover the full hydraulic fracturing treatment.

In the ensuing illustrative examples, we use the following three models with unknown parameters $\boldsymbol{m}$, which have analytical expressions for the tilts:

- a penny–shaped fracture of radius R under constant pressure p in an infinite elastic medium [7] $\boldsymbol{m} = (\phi,\, \theta,\, R,\, p)$ (model $\mathcal{M}_1$),
- a square Displacement Discontinuity of half-length a and opening δ in an infinite medium [15]: $\boldsymbol{m} = (\phi,\, \theta,\, \psi,\, a,\, \delta)$ (model $\mathcal{M}_2$),
- a Displacement Discontinuity Singularity with an intensity equal to the volume of the fracture $\mathcal{V}$: $\boldsymbol{m} = (\phi,\, \theta,\, \mathcal{V})$, (model $\mathcal{M}_3$).

All fracture models can have any orientation in space, and this orientation is defined by Euler angles. We assume that the center of the model coincides with the known location of the injection point.

3. BAYESIAN MODEL SELECTION

The posterior probability of model $\mathcal{M}_k$, after the data have been observed, can be written using Bayes' rule as

$$p(\mathcal{M}_k|\boldsymbol{d}) = \frac{p(\boldsymbol{d}|\mathcal{M}_k)p(\mathcal{M}_k)}{p(\boldsymbol{d})}. \tag{4}$$

The denominator $p(\boldsymbol{d})$ in eqn.(4) denotes the probability that the data have been observed, and is a constant which is taken to normalize the expression as $p(\boldsymbol{d}) = \sum_k p(\boldsymbol{d}|\mathcal{M}_k)p(\mathcal{M}_k)$. $p(\mathcal{M}_k)$ is the prior probability of model $\mathcal{M}_k$ and $p(\boldsymbol{d}|\mathcal{M}_k)$ is the marginal probability of the data for model $\mathcal{M}_k$. This last quantity involves an integral over the entire parameter space for the given model $\mathcal{M}_k$:

$$p(\boldsymbol{d}|\mathcal{M}_k) = \int\int p(\boldsymbol{d}|\boldsymbol{m}_k, \sigma_k)p(\boldsymbol{m}_k, \sigma_k)\ \mathrm{d}\boldsymbol{m}_k\ \mathrm{d}\sigma_k \tag{5}$$

In expression (5), the conditional probability $p(\boldsymbol{d}|\boldsymbol{m}_k, \sigma_k)$ is the probability that the data $\boldsymbol{d}$ were generated by model $\mathcal{M}_k$ with parameters $\boldsymbol{m}_k, \sigma_k$, and is usually called the Likelihood function for parameter estimation problem. The probability $p(\boldsymbol{m}_k, \sigma_k)$ is the prior probability on the model parameters and model variance for model $\mathcal{M}_k$. We shall refer to $\pi(\boldsymbol{m}_k, \sigma_k|\boldsymbol{d}) = p(\boldsymbol{d}|\boldsymbol{m}_k, \sigma_k)p(\boldsymbol{m}_k, \sigma_k)$ as the Bayesian posterior distribution for model $\mathcal{M}_k$.

To compare two models, we compute the ratio of their posterior probability as in eqn.(4):

$$\frac{p(\mathcal{M}_1|\boldsymbol{d})}{p(\mathcal{M}_2|\boldsymbol{d})} = \underbrace{\left[\frac{p(\boldsymbol{d}|\mathcal{M}_1)}{p(\boldsymbol{d}|\mathcal{M}_2)}\right]}_{B_{12}} \left[\frac{p(\mathcal{M}_1)}{p(\mathcal{M}_2)}\right]. \tag{6}$$

The first factor B_{12} is the so–called Bayes factor: it is the ratio of the marginal probability of the data for the models $\mathcal{M}_1$ and $\mathcal{M}_2$. The second factor is the ratio of the model prior probability, and in many cases will be set to unity, so model 1 and 2 are equiprobable prior choices. The main quantity of interest is thus the Bayes factor B_{12}. As noted in [14, 9], when the Bayes factor B_{12} is greater than 10, the data clearly favours the the model $\mathcal{M}_1$ over the model $\mathcal{M}_2$. When $1 < B_{12} < 5$, both models can be though to consistently reproduce the data. Finally for $B_{12} < 1$, the data favor the model $\mathcal{M}_2$ over the model $\mathcal{M}_1$ with the same restrictions if one looks at B_{21}.

In our case the set of models is discrete, so the general solution of the model selection problem can be split into two parts. First, for each model $\mathcal{M}_k$, from the posterior pdf $\pi(\boldsymbol{m}_k, \sigma_k|\boldsymbol{d})$, we estimate the marginal probability $p(\boldsymbol{d}|\mathcal{M}_k)$ of the data using eqn.(5). Second, the full set of Bayes factors are computed in order to rank the different models. The main difficulty is to compute the marginal probability of the data for model $\mathcal{M}_k$, which involves an integration over the entire parameter space eqn.(5).

3.1 Definition and solution for a given model

In this section, we define all the required probability density functions for a given model $\mathcal{M}_k$, but drop the reference to k for clarity. The likelihood is taken as a normal probability function for the error in eqn.(3):

$$p(\boldsymbol{d}|\boldsymbol{m}, \sigma) = \frac{1}{(2\pi\sigma^2)^{N/2}} \exp\left[-\frac{1}{2\sigma^2}(\boldsymbol{d} - \boldsymbol{g}(\boldsymbol{m}))^T(\boldsymbol{d} - \boldsymbol{g}(\boldsymbol{m}))\right]. \tag{7}$$

Assuming that the prior on the model parameters $p(\boldsymbol{m}, \sigma)$ is independent of the prior on the noise variance, we have

$$p(\boldsymbol{m}, \sigma) = p(\boldsymbol{m})p(\sigma) \tag{8}$$

and we choose normal forms for the prior on the model parameters:

$$p(\boldsymbol{m}) = \frac{1}{(2\pi)^{d/2}|\boldsymbol{C}_p|^{1/2}} \exp\left[-\frac{1}{2}(\boldsymbol{m}_p - \boldsymbol{m})^T\boldsymbol{C}_p^{-1}(\boldsymbol{m}_p - \boldsymbol{m})\right]. \tag{9}$$

Here $\boldsymbol{m}_p$ is a vector of prior means for the d parameters of model $\mathcal{M}$, and $\boldsymbol{C}_p$ is the corresponding prior covariance matrix. This matrix is diagonal in our case as all model parameters are supposed independent. (In the Hydraulic fracturing case, the fracture orientation is related to the initial stress, whereas the length is related to the injected volume). As the variance should be a positive scale number, we choose an uninformative Jeffrey's prior:

$$p(\sigma) = 1/\sigma. \tag{10}$$

The goal is now to characterize the posterior pdf $\pi(\boldsymbol{m}, \sigma|\boldsymbol{d}) = p(\boldsymbol{d}|\boldsymbol{m}, \sigma)p(\boldsymbol{m})p(\sigma)$ and compute the marginal probability of the data for the given model (eqn.5). In most cases this requires a high dimensional integration and is therefore often untractable numerically. However, several methods can be used in order to obtain an approximation to the integral, e.g. the Laplace approximation, and with further assumptions, the BIC approximation. We refer to [9, 14] for a complete discussion, and derivation, of the different methods related to the estimation of the marginal probability of the data.

The first step is to approximate the posterior pdf by a normal multivariate distribution around its mode. Introducing the vector $\boldsymbol{z} = (\boldsymbol{m}, \sigma)$ of dimension $d+1$, and denoting the pdf mode as $\tilde{\boldsymbol{z}}$, we write:

$$\pi(\boldsymbol{m}, \sigma|\boldsymbol{d}) = \pi(\boldsymbol{z}|\boldsymbol{d}) \approx \pi(\tilde{\boldsymbol{z}}|\boldsymbol{d}) \exp\left(-\frac{1}{2}(\boldsymbol{z}-\tilde{\boldsymbol{z}})^T \tilde{\boldsymbol{C}}^{-1}(\boldsymbol{z}-\tilde{\boldsymbol{z}})\right) \tag{11}$$

where $\tilde{\boldsymbol{C}}$ is the posterior covariance matrix at the mode $\tilde{\boldsymbol{z}}$. The integral (5) can then be estimated using the so-called Laplace approximation for integrals (see [13] for details):

$$p(\boldsymbol{d}|\mathcal{M}) \approx \pi(\tilde{\boldsymbol{z}}|\boldsymbol{d})(2\pi)^{(d+1)/2}|\tilde{\boldsymbol{C}}|^{1/2} \tag{12}$$

A further approximation of eqn.(12) leads to the so-called BIC approximation (Bayesian Information Criterion). This approximation is valid for large samples and gives (again see [13] for a complete discussion):

$$\log p(\boldsymbol{d}|\mathcal{M}) \approx \log \pi(\tilde{\boldsymbol{z}}|\boldsymbol{d}) - \frac{d+1}{2}\log N + O(1) \tag{13}$$

The error associated with such approximation is of order 1, but is commonly believed to be of the same order for different models so that it is still possible to use it in order to compare several models. This approximation appears somewhat crude, but has the advantage of not requiring an explicit estimate of the posterior covariance matrix. Finally, an alternative way to characterizes the posterior model parameter pdf is by using a Markov Chain Monte Carlo (MCMC) algorithm. We refer to [14] and, in general [6] for a discussion of this approach.

In practice, the mode of the posterior pdf is found by minimizing the functional $\mathcal{J}(\boldsymbol{z}) = -\log \pi(\boldsymbol{m}, \sigma|\boldsymbol{d})$ with respect to the variables $\boldsymbol{z} = (\boldsymbol{m}, \sigma)$. In our case, in order to ensure that the variance σ remains positive during the optimization, we perform a re parametrization by taking $\alpha = \log \sigma$ as unknown. We therefore have the prior $p(\alpha) = 1$ and the functional can be written as

$$\begin{aligned} \mathcal{J}(\boldsymbol{z} = (\boldsymbol{m}, \alpha))) &= \frac{N+d}{2}\log(2\pi) + \frac{1}{2}\log|\boldsymbol{C}_p| + N\alpha \\ &+ \frac{1}{2}\exp(-2\alpha)(\boldsymbol{d}-\boldsymbol{g}(\boldsymbol{m}))^T(\boldsymbol{d}-\boldsymbol{g}(\boldsymbol{m})) + \frac{1}{2}(\boldsymbol{m}_p-\boldsymbol{m})^T\boldsymbol{C}_p^{-1}(\boldsymbol{m}_p-\boldsymbol{m}) \end{aligned} \tag{14}$$

The minimum $\tilde{\boldsymbol{z}}$ of $\mathcal{J}(\boldsymbol{z})$ corresponds to the mode of the posterior of the model parameter $\pi(\tilde{\boldsymbol{z}}|\boldsymbol{d})$. The Hessian matrix $\tilde{\boldsymbol{H}}$ of $\mathcal{J}(z)$ at the minimum is directly related to the covariance matrix $\tilde{\boldsymbol{C}} = \tilde{\boldsymbol{H}}^{-1}$. This covariance, or Hessian matrix, can be obtained using a Taylor expansion around $\boldsymbol{z}$ (see [16] for details). Then, for the particular model chosen, we can obtain an approximation of $p(\boldsymbol{d}|\mathcal{M})$ via (12) (Bayes Factor) or (13) (BIC).

For our particular problem and the model used, the functional $\mathcal{J}(\boldsymbol{z})$ has proved to be relatively smooth and convex, and the normal approximation of the posterior generally appears very good in salient cross-sections of the log–posterior. The minimization is performed via a quasi-Newton algorithm (BFGS with a Wolfe line search), which is computationally very efficient but will only converge to a local minima. In order to globalize the algorithm, the optimization is performed starting from several randomly chosen initial guesses for the parameters $\boldsymbol{z}$.

The significance and use of prior probability distributions has been a topic of much debate in Bayesian estimation. An important issue is the appropriate specification of uninformative priors: we discuss here a few important implications for the posterior in model selection problems (see [3] for details). As can be seen from the normal form of the prior on model parameters, one can seemingly force an uninformative prior on model parameters by setting the scale of the prior covariance matrix entries $\boldsymbol{C}_p$ to a very large positive number. Such a choice should be avoided. In the scope of model selection, large $\boldsymbol{C}_p$ have a direct influence on the value of the mode of the posterior probability via the terms in $|\boldsymbol{C}_p|$. Such non-informative priors will always heavily favour the model with the least number of parameters, when the Bayes factor are computed. This is the so-called Lindley's Paradox. As a rule of thumb, in order to input uninformative priors, it is practical to take variances on the prior model parameters value of not more than one order of magnitude greater than the prior mean.

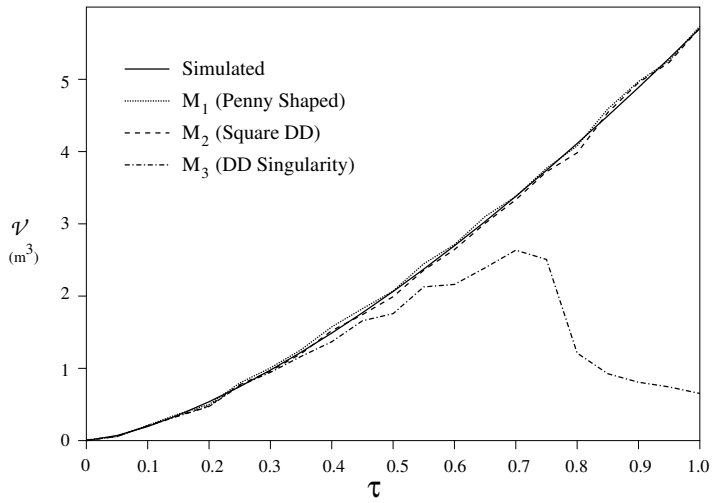

Figure 3. Synthetic example: Estimated fracture volume $\mathcal{V}$ at different times τ during the simulated fracturing treatment.

4. EXAMPLES

We now apply this model selection approach to two example problems: a synthetic data set, and a field example. We have to note that despite the fact that the hydraulic fracture evolves during a treatment, the models used here are static, *not* propagation models. Nevertheless, the inverse problem can be sequentially repeated in time in order to furnish an estimation of the hydraulic fracture growth.

4.1 A synthetic example

We have simulated the tilt data corresponding to the propagation of a penny-shaped hydraulic fracture in the so-called toughness dominated regime of propagation [4]. In this regime, the propagation of the hydraulic fracture, located in a full space, is self-similar and the pressure inside the fracture is homogeneous. The evolution of the fracture radius and pressure are given by power laws of time:

$$R(\tau) = \bar{L}_k \gamma_{ko} \tau^{2/5} \quad p(\tau) = \bar{\epsilon}_k E' \Pi_{ko} \tau^{-1/5} \tag{15}$$

where γ_{ko} and Π_{ko} are constants [4]. The dimensionless time is defined as $\tau = \frac{t}{t_c}$ and the characteristic time t_c is related to the injection rate Q_o, plane strain Young's Modulus E', fracture toughness K' and fracturing fluid viscosity μ': $t_c = \left(\dfrac{\mu'^{1/5} Q_o^3 E'^{13}}{K'^{18}} \right)^{1/2}$. The characteristic length scale $\bar{L}_k$ and dimensionless number $\bar{\epsilon}_k$ are given by $\bar{L}_k = \dfrac{E'^3 Q_o \mu'}{K'^4}$ and $\bar{\epsilon}_k = \left(\dfrac{K'^6}{E'^5 Q_o \mu'} \right)^{1/2}$ respectively. In order to simulate the data, we have used here $\bar{L}_k = 50$ and $\bar{\epsilon}_k = 10^{-3}$. The array of measurements consists of 13 tiltmeter stations (26 tilt data) spatially located in a plan approximatively 75 meters above the center of the fracture. The orientation of the fracture remains constant with a dip θ of 5° and a strike of 80° with respect to North. We simulate the tilt data at different dimensionless times $\tau_i = \tau_{i-1} + 0.05$ from 0 to 1. A Gaussian noise component of standard deviation $\sigma_{input} = 0.5\mu$ radians is added to the tilt data vectors at each time.

The evolution of the fracture dimensions and locations of the tiltmeters have been taken such that for small dimensionless time τ (i.e: small fracture), the measurements are located in the far field of the fracture (distance to the fracture greater than $4R$). As time increases, the radius of the fracture R gets larger and the measurements become "near field". From the length scales resolution limit previously discussed [11], we expect that at small time we will resolve the fracture volume but not the fracture dimensions. At large time, we will be able to obtain the fracture dimensions. The far-field/near-field limit has been computed and the transition from far-field to near-field occur at a dimensionless time $\tau \approx 0.3$.

An inversion is performed for all τ_i using the three different models defined previously: penny-shaped ($\mathcal{M}_1$, 4 parameters: radius, pressure, orientation), square DD ($\mathcal{M}_2$, 5 parameters: length, opening, orientation), DD Singularity ($\mathcal{M}_3$, 3 parameters: volume, orientation). We note that the inversion at different times are completely independent: the models are static. We seek to estimate which model better

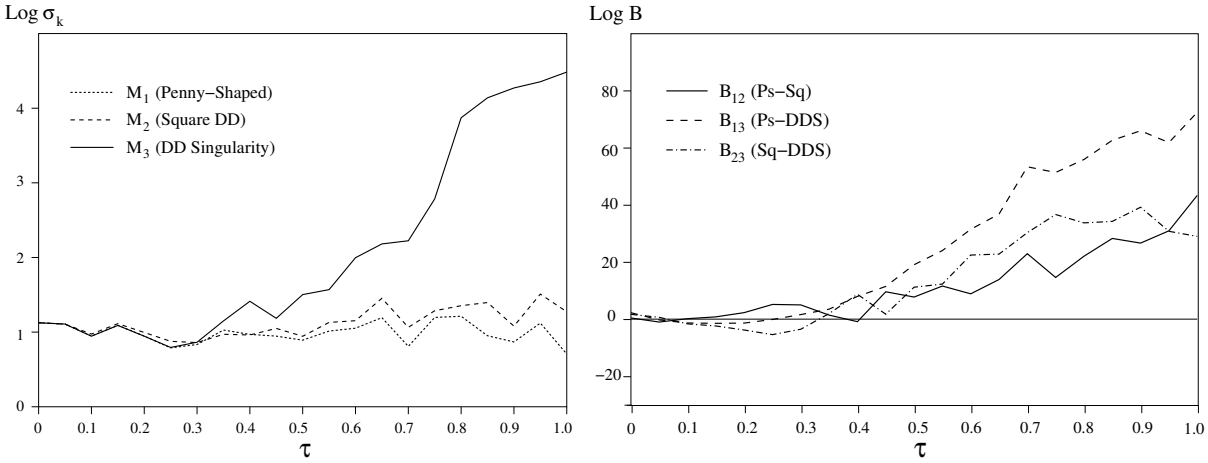

Figure 4. Synthetic example: estimated Modelling error standard deviation vs time (left) and Bayes factors for the different models. Model $\mathcal{M}_3$ is the most probable at small time, Model $\mathcal{M}_1$ at large time.

explains the data at a given time, and this procedure is repeated for all τ_i in the interval $[0, 1]$. The same prior probability on the fracture orientation is taken for all models: $\phi_{\text{prior}} = 80°$, std deviation $= 15°$ and $\theta_{\text{prior}} = 0°$, std deviation $= 15°$. The prior on the length scales or volume are taken uninformative with a variance about one order of magnitude greater than the prior mean value. This choice avoids a too strongly uninformative prior and the associated Lindley paradox effects when the Bayes factor are estimated.

Results First of all, we can see in Figure 3 the estimation of the fracture volume obtained for the three models at different times during the simulated treatment. As expected, the "true" model $\mathcal{M}_1$ always perfectly estimates the fracture volume. However, at small time ($\tau < 0.3$), the estimated values of the fracture radius and net pressure do not coincide with the simulated ones defined by eqn.(15). In the case of far-field measurement, the length scales of the Penny-shaped model are not estimated independently. For time above $\tau \approx 0.3$ (e.g. near-field measurement), the fundamental DD Singularity (model $\mathcal{M}_3$) gives a wrong estimate of the fracture volume. Thus for near-field measurements, the DD Singularity model is clearly inadequate. In a sense, we recover the far-field / near-field limit on the resolution of fracture dimensions [11]. A further verification of the resolution limit is given by the fact that the length scales of the "true" model ($\mathcal{M}_1$) are exactly recovered for time above $\tau \approx 0.3$.

Figure 4 shows the evolution of the Bayes factors B_{12}, B_{13}, B_{23} and the model noise standard deviation as the fracture grows. Interestingly, at early time ($\tau < 0.3$), the data favours the DD singularity model over the penny-shaped and square DD model as $\log B_{23}$ and $\log B_{13}$ are around -3. The identified noise standard deviation are similar for the three models at early time and close to the noise standard deviation input on the simulated data ($\sigma_{input} = 0.5\mu$ radians). For $\tau > 0.3$, the penny-shaped and square DD models start to better resolve the data: $\log B_{23}$ and $\log B_{13}$ are largely positive. The estimated model noise variance for these two models ($\mathcal{M}_1$ and $\mathcal{M}_1$) are also lower than the DD Singularity at large time (Figure 4). The predicted fracture volume from the two models remains very close to the simulated one (Figure 3) whereas the DD singularity clearly mis–estimates the fracture volume.

It is interesting to note that the square DD model $\mathcal{M}_2$ furnishes an accurate estimation of fracture volume even for large times, when the recorded tilts sample the near field of the fracture. The Bayes factor B_{12} between model $\mathcal{M}_1$ and $\mathcal{M}_2$ does not increase as fast as the other two, but still rises quickly above 10^3. The Penny shaped model better explains the data than the square DD model at large time. This is to be expected, as it is the "true" model for this synthetic case. However, such conclusions could not have been drawn from the estimation of fracture volume alone (Figure 3). Further, the estimated noise standard deviation for the true model ($\mathcal{M}_1$) is always of the same order of magnitude as the input noise for all time ($\sigma_{input} = 0.5\mu$ radians). This indicates that this model is consistent with the data. In comparison, the estimated noise standard deviation is appreciably larger than the input noise standard deviation for the square DD model at large time.

4.2 Field example

We now turn to the analysis of measured tilt data obtained during a field hydraulic fracture experiment, which comprised the injection of a 10 m^3 water over a 30 minute period. This full-scale hydraulic

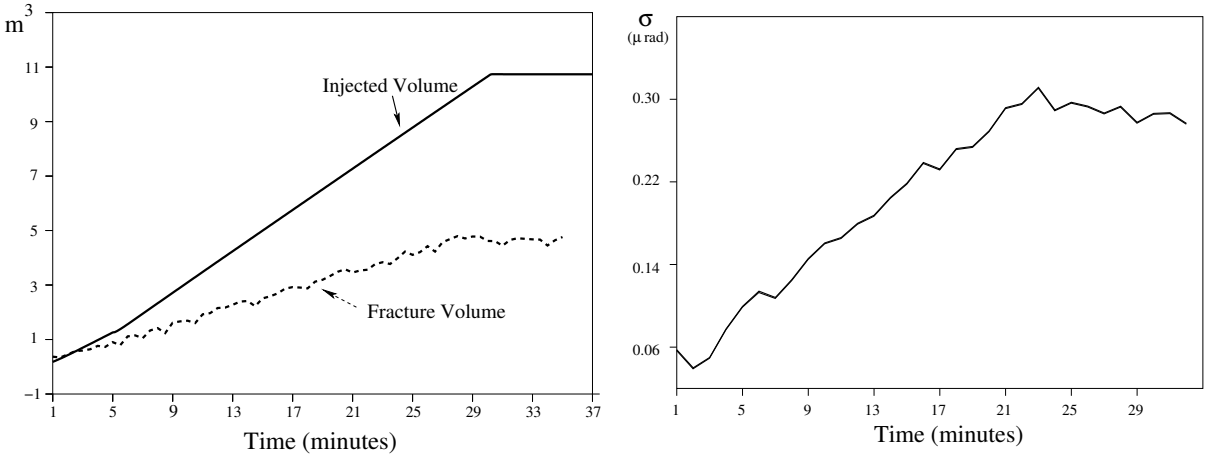

Figure 5. Field Data example: Estimated Fracture volume and injected fluid volume (left), estimated model error standard deviation (right) for the DD Singularity model ($\mathcal{M}_3$).

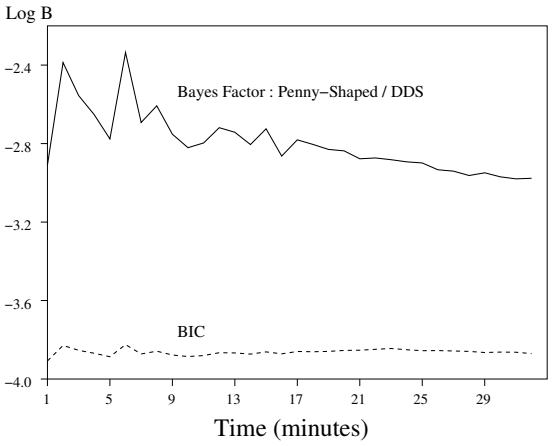

Figure 6. Field Data example: Bayes factor and BIC comparing the penny-shaped and DD Singularity models. The data favors the DD Singularity model $\mathcal{M}_3$ at all time.

fracturing experiment was performed by CSIRO Petroleum at a mine located in New South Wales, Australia. The data was logged by an array of 13 tiltmeters positioned about 75 metres above the hydraulic initiation point. A full description of this experiment can be found in [10]. We are interested here in the result of the Bayesian model selection. The data have been analyzed using two models: penny-shaped ($\mathcal{M}_1$) and DD Singularity ($\mathcal{M}_3$). No apriori information on the volume of the fracture, or the fracture radius in the case of $\mathcal{M}_1$, are taken into account. However, knowledge of the state of regional stresses at the site has enabled us to introduce a relatively weak prior on the fracture orientation as follows (prior value and associated prior standard deviation): Azimuth $\phi_{\text{prior}} = 80°$ std deviation $\sigma = 25°$ and Dip $\theta_{\text{prior}} = 0°$, std deviation $\sigma = 15°$.

Both models furnish exactly the same estimate of fracture volume and orientation throughout the treatment period. Some of the results for the DD Singularity model are displayed in Figure 5. The estimated values of the Euler angles are approximately constant during the treatment: $\theta = 15°$, $\phi = 70°$. The estimated model error standard deviation increases during the treatment and asymptotes to around 0.3μrad. This value is larger than the noise standard deviation of the signal measured by the tiltmeter station ($\approx 0.1\mu$rad) which indicates that the models do not entirely reproduce the data (heterogeneity of the rock mass etc.). The fit at a particular tiltmeter station can be seen in Figure 2. In the case of the penny-shaped model, the estimated dimensions (radius, net pressure) are always highly correlated. This indicates a problem of length–scale resolution. The evolution of the Bayes Factor between the 2 models B_{13} as well as the value for the BIC approximation are displayed in Figure 6. Both clearly favor the DD singularity model throughout the whole treatment: $\log B_{13}$ negative. We can conclude that, for this experiment, the created fracture never grew long enough for the tiltmeters to detect a near-field effect.

5. CONCLUSIONS

In this paper, we have applied Bayesian model selection ideas to the hydraulic fracture imaging problem using tiltmeter measurements. This analysis incorporated an unknown error variance in the framework of the normal probability model. The modeling error can be quantified by comparing the estimated noise modeling error variance to the recorded measurement noise. We have demonstrated the use of Bayes factor to rank a suite of possible models for both synthetic and field data. For this particular inverse problem, the Bayes factors reveal the near-field/far-field resolution limit for the fracture dimensions. This is of particular interest for field applications where the expected fracture length, and therefore the resolution limit, is poorly known.

REFERENCES

1. S. Andrieux, A. Ben Abda and H. D. Bui, Reciprocity principle and crack identification. *Inverse Problems* (1999) **15**, 59–65.

2. J. L. Beck and K. Yuen, Model selection using response measurements: Bayesian probabilistic approach. *J. Eng. Mech. ASCE* (2004) **130**(2), 192–203.

3. D.G.T. Denison, C.C. Holmes , B.K. Mallick and A.F.M. Smith, *Bayesian Methods for Non-Linear Classification and Regression*, Wiley & Sons, New York, 2002.

4. E. Detournay, Propagation regimes of fluid-driven fractures in impermeable rocks. *Int. J. Geomechanics* (2004) **4**(1), 1–11.

5. M.J. Economides and K.G. Nolte, (Eds.) *Reservoir Stimulation*, John Wiley & Sons, Chichester UK, 3rd edition, 2000.

6. W.R. Gilks, S. Richardson and D.J. Spiegelhalter, *Markov Chain Monte Carlo in Practice*, Chapman & Hall, London, 1996.

7. A. E. Green, On Boussinesq's problem and penny-shaped cracks. *Proc. Cambridge Phil. Soc.* (1948) **45**(2), 251–257.

8. D.A. Hills, P.A. Kelly, D.N. Dai and A.M. Korsunsky, *Solution of Crack Problems*, Kluwer Academic Publishers, Dordretch, 1996.

9. R.E. Kass and A.E. Raftery, Bayes factors. *J. American Statistical Soc.* (1995) **90**(430), 773–795.

10. B. Lecampion, R. Jeffrey and E. Detournay, Real-time estimation of fracture volume and hydraulic fracturing treatment efficiency, In *Proc. of the 6th North America Rock Mechanics Symposium, Gulf Rocks 2004*, Paper ARMA/NARMS 04–519, 2004.

11. B. Lecampion, R. Jeffrey and E. Detournay, Resolving the geometry of hydraulic fractures from tilt measurements, accepted for publication in *Pure and Applied Geophysics*, 2005.

12. A. Malinverno, Parsimonious Bayesian Markov chain Monte Carlo inversion in a nonlinear geophysical problem. *Geophys. J. Int.* (2002) **151**, 675–688.

13. A. Raftery, Bayesian model selection in social research (with discussion), In *Sociologial Methodology* (ed. P.V. Marsden), Jossey-Bass, San Francisco, 1995.

14. A. Raftery, *Markov Chain Monte Carlo in Practice*, chapter Hypothesis testing and model selection, Chapman & Hall, London, 1996, pp 163–187.

15. L. Rongved, Dislocation over a bounded plane area in an infinite solid. *ASME J. Appl. Mech.* (1957) **24**, 252–254.

16. A. Tarantola and B. Valette, Inverse Problems = Quest for information. *J. Geophys.* (1982) **50**, 159–170.